

# Are galaxies with AGN a transition population?

P. B. Westoby<sup>\*</sup>, C. G. Mundell and I. K. Baldry

*Astrophysics Research Institute, Liverpool John Moores University, Twelve Quays House, Egerton Wharf, Birkenhead, CH41 1LD, UK*

Accepted 2007 September 22. Received 2007 August 28; in original form 2007 June 28

## ABSTRACT

We present the results of an analysis of a well-selected sample of galaxies with active and inactive galactic nuclei from the Sloan Digital Sky Survey, in the range  $0.01 < z < 0.16$ . The SDSS galaxy catalogue was split into two classes of active galaxies, Type 2 AGN and composites, and one set of inactive, star-forming/passive galaxies. For each active galaxy, two inactive control galaxies were selected by matching redshift, absolute magnitude, inclination, and radius. The sample of inactive galaxies naturally divides into a red and a blue sequence, while the vast majority of AGN hosts occur along the red sequence. In terms of H $\alpha$  equivalent width, the population of composite galaxies peaks in the valley between the two modes, suggesting a transition population. However, this effect is not observed in other properties such as colour-magnitude space, or colour-concentration plane. Active galaxies are seen to be generally bulge-dominated systems, but with enhanced H $\alpha$  emission compared to inactive red-sequence galaxies. AGN and composites also occur in less dense environments than inactive red-sequence galaxies, implying that the fuelling of AGN is more restricted in high-density environments. These results are therefore inconsistent with theories in which AGN host galaxies are a ‘transition’ population. We also introduce a systematic 3D spectroscopic imaging survey, to quantify and compare the gaseous and stellar kinematics of a well-selected, distance-limited sample of up to 20 nearby Seyfert galaxies, and 20 inactive control galaxies with well-matched optical properties. The survey aims to search for dynamical triggers of nuclear activity and address outstanding controversies in optical/IR imaging surveys.

**Key words:** galaxies: active – galaxies: Seyfert – galaxies: star-forming – galaxies: evolution.

## 1 INTRODUCTION

Active Galactic Nuclei (AGN) have long been considered a curiosity in their own right (Schmidt 1963; Lynden-Bell 1969; Blandford & Rees 1974), but are now recognised to be integral to galaxy formation and evolution. At early cosmological epochs, gas-rich galaxies are thought to form and collide in violent mergers (Mihos & Hernquist 1996), triggering vast bursts of star formation, and fuelling supermassive black holes in their cores (Kriek et al. 2006). Recent simulations of isolated and merging galaxies by Springel et al. (2005) have incorporated feedback from star formation and black-hole accretion, and find that once an accreting supermassive black hole (SMBH) has grown to some critical size, the AGN feedback terminates its growth as a large fraction of the remaining nuclear gas is driven out by the powerful quasar.

In the current epoch, the peak of the quasar era is

over and the galaxy merger rate has declined (Struck 1997). Nevertheless, at least 20% of today’s galaxies show scaled-down quasar activity in their centres, and direct measurements of active and inactive galaxy dynamics have revealed a tight correlation between the central black-hole mass and host galaxy stellar velocity dispersion or bulge mass. This  $M_{\bullet} - \sigma$  relation (Gebhardt et al. 2000; Merritt & Ferrarese 2001) points to an intimate link between host galaxy evolution and central black-hole growth, suggesting that all bulge-dominated galaxies today harbour dead quasars and that a lack of nuclear activity cannot be attributed to the absence of a central black hole. Therefore, given the ubiquity of supermassive black holes, what determines the degree of nuclear activity in today’s galaxies and what role is played by the host galaxy in triggering and fuelling their dormant black holes remain open issues.

Previously, studies of nearby active galaxies were based on small galaxy samples, like the CfA Seyfert Sample (Huchra & Burg 1992), the 12 Micron Active Galaxy Sample (Rush et al. 1993) and the Ho et al. (1995) galaxy sam-

<sup>\*</sup> E-mail: pbw@astro.livjm.ac.uk

ple of approximately 486 galaxies covering a range of activity types. Now, however, the standard has been set by the Sloan Digital Sky Survey (SDSS), from which a range of useful samples of both active and inactive galaxies can be selected in a well-defined, uniform way.

The SDSS (York et al. 2000) provides, for the first time, 5-band photometry and spectroscopy of many thousands of low redshift AGN (Kauffmann et al. 2003c; Hao et al. 2005a), enabling constraints to be placed on galaxy and AGN evolution over a wide range of galaxy masses, and acts as the definitive supporting data to all detailed follow-up galaxy studies. Initial investigations into the growth and evolution of black holes using these databases have yielded contrasting results — the origin of the correlation between galaxy bulge and central black-hole masses is hotly debated in particular.

Heckman et al. (2004) find that the majority of present-day accretion occurs onto  $10^8$  solar-mass black holes in moderate mass galaxies, suggesting that bulge and black-hole evolution is still tightly coupled today, and that the evolution of AGN luminosity functions is driven by a decrease in the mass scale of accreting black holes. In contrast, the Hao et al. (2005b) study of about 3000 SDSS AGN concludes that evolution in AGN luminosity functions is driven by evolution in the Eddington ratio, rather than black-hole mass. Meanwhile, Grupe & Mathur (2004) and Mathur & Grupe (2005) use a sample of 75 X-ray selected AGN to argue that black holes in Narrow Line Seyfert 1 galaxies in particular, grow by accretion in well-formed bulges to produce the  $M_{\bullet} - \sigma$  relation over time, refuting theories for the origin of black-hole / bulge relations in which black-hole mass is a constant fraction of bulge mass at all epochs or in which bulge growth is controlled by AGN feedback (King 2003; Ferrarese 2002; Kriek et al. 2006). The subclass of NLS1s has been further explored more recently by Komossa & Xu (2007), who find that NLS1s are accreting at a rate higher than the Eddington rate, confirming that their BHs must be growing. They suggest that either NLS1 galaxies evolve into Broad Line Seyfert 1 (BLS1) galaxies with respect to their black hole mass distribution, which would require some change in the bulge properties, possibly due to feedback, or that NLS1s are just low-mass extensions of BLS1 galaxies, and the high accretion rate could just be caused by a relatively short-lived accretion phase.

Another characteristic revealed by large automated surveys such as the SDSS, is that the galaxy population is found to be bimodal in colour (Lilly et al. 1995; Strateva et al. 2001), with it now being more natural to describe a galaxy as being on the “red sequence” or “blue sequence”, rather than being “early type” or “late type” (Baldry et al. 2006). A key goal of galaxy evolution theory is then to explain the colour bimodality of galaxies, the relationships within each sequence, and where active hosts fit into this picture. Therefore, the understanding of galaxy formation and evolution processes necessitates full inclusion of AGN and their hosts.

Recently efforts have been made to try to understand where AGN host galaxies fall in colour-magnitude space. The red sequence consists of mainly massive, passively evolving galaxies, while the majority of galaxies show blue colours, attributed to ongoing star formation. The two sequences are separated by a relatively narrow valley in colour space.

The emerging consensus is that intense star formation is fuelled by galaxy mergers at high redshift, which forms massive bulges, and at some point the star formation ceases, resulting in the galaxy migrating from the blue sequence to the red sequence. AGN have been singled out as the mechanism for star-formation quenching, leading to suggestions that AGN should occupy a distinct, ‘transition’ region, of the colour-magnitude diagram (CMD). However this does not necessarily have to be the case, as the resulting galaxy could just be bluer due to increased star-burst activity, or redder due to enhanced dust (e.g., Luminous Infra-Red Galaxies), or some combination of the original colours of the merging galaxies. Young stellar populations and nuclear starbursts are therefore also important components in the dynamics of nuclear activity (González Delgado et al. 1998; Sarzi et al. 2007).

Nandra et al. (2007) studied the colour-magnitude relation for a sample of 50 X-ray selected AGN from the AEGIS survey (All-wavelength Extended Groth strip International Survey), in the range  $0.6 < z < 1.4$ . They conclude that AGN fall on the red sequence or on the red edge of the blue sequence, with many in between these two modes.

Martin et al. (2007) further explored the idea of a ‘transition’ region by exploiting the separation of the blue and red sequences in the  $UV - r$  colour-magnitude diagram. Using a sample of UV selected galaxies from the GALEX Medium Imaging Survey, along with SDSS data, they explored the nature of galaxies in the transition zone. The AGN fraction of their sample was found to peak in the transition zone, and they also found circumstantial evidence that star-formation quenching rates were higher in higher luminosity AGN.

Higher image quality than the SDSS is provided by the Millennium Galaxy Catalogue (MGC; Liske et al. 2003; Cross et al. 2004), which has obtained redshifts for 10 095 galaxies to  $B < 20$  mag, covering  $37 \text{ deg}^2$  of equatorial sky. The MGC study of galaxy bimodality was in the colour-structure plane, (Driver et al. 2006; hereafter D06) and expressed a contrasting theory for the bimodality. The MGC survey has sufficient resolution to achieve reliable bulge-disc decomposition (Allen et al. 2006), and in separating out the two components, D06 claim that galaxy bimodality is caused by the bulge-disc nature of galaxies, and not by two distinct galaxy classes at different evolutionary stages. In this case, they show that the bulge-dominated, early-type galaxies populate one peak and the bulge-less, late-type galaxies occupy the second. The early- and mid-type spirals sprawl across and between the peaks. They also propose that the reason for the dual structure of galaxies is due to galaxy formation proceeding in two stages; first, there is an initial collapse phase, which forms the centrally concentrated core and a black hole, and second, there is the formation of a planar rotating disc caused by accretion of external material building up the galaxy disk.

In this paper, we present the properties of a magnitude-limited sample of “active” and “inactive” galaxies carefully selected from the SDSS, which also acts as the parent sample for detailed followup studies using the IMACS-IFU on the Magellan 6.5m telescope. Our sample selection is described in §3, the sample properties in §4, and implications of these properties in §5. We conclude by introducing the Magellan survey, which is now underway.

## 2 THE SLOAN DIGITAL SKY SURVEY

The SDSS (York et al. 2000; Stoughton et al. 2002) is an imaging and spectroscopic survey, which, when completed, will provide detailed optical images covering more than a quarter of the sky and a 3-dimensional map of about a million galaxies and quasars. The survey uses a dedicated 2.5m telescope at Apache Point Observatory, New Mexico, equipped with a large format mosaic CCD camera — 30 CCDs in six columns and five rows — to image in five optical bands;  $u$ ,  $g$ ,  $r$ ,  $i$  and  $z$ , with effective wavelengths of 3550, 4670, 6160, 7470 and 8920 Å (Fukugita et al. 1996; Gunn et al. 1998).

The images are calibrated photometrically (Hogg et al. 2001) and astrometrically (Pier et al. 2003) using a separate 0.5-m telescope, and reduced using a pipeline **photo** that measures the observing conditions, and detects and measures objects. In particular, **photo** produces various types of magnitude including ‘Petrosian’, the summed flux in an aperture that depends on the surface-brightness profile of the object. The magnitudes are Galactic extinction-corrected using the dust maps of Schlegel et al. (1998). Details of the imaging pipelines are given by Stoughton et al. (2002).

The main telescope is also equipped with two double fibre-fed spectrographs, covering a wavelength range of 3800–9200 Å, over 4098 pixels, with a resolution of  $\lambda/\Delta\lambda \sim 1800$ . Once a sufficiently large area of sky has been imaged, the data are analysed using ‘targeting’ software routines that determine the objects to be observed spectroscopically. The targets are then assigned to plates, each with 640 fibres, using a tiling algorithm (Blanton et al. 2003a). The main restriction is that two fibres cannot be placed within 55'' on the same plate.

Spectra are typically taken using three 15-minute exposures in moderate conditions (the best conditions are used for imaging). The signal-to-noise ratio ( $S/N$ ) is typically 10 per pixel (1–2Å) for galaxies. The pipeline **spec2d** extracts, and flux- and wavelength-calibrates the spectra.

## 3 SAMPLE SELECTION

We start with the galaxy catalogue from the SDSS Fourth Data Release (DR4; Adelman-McCarthy et al. 2006), as distributed by the MPA Garching group. The catalogue<sup>1</sup> (Kauffmann et al. 2003a; Brinchmann et al. 2004; Tremonti et al. 2004) contains photometric and follow-up spectroscopic data for all objects spectroscopically classified as galaxies with Petrosian  $r$ -band magnitudes less than 17.77. The catalogue does not include objects classified as ‘quasars’ by the SDSS spectral classification algorithm. Broad emission-line galaxies (‘Type 1’ Seyferts) are therefore generally excluded from the MPA catalogue, although there are still some Type 1 Seyferts remaining if their spectra contain a significant fraction of stellar light. Galaxies with a velocity dispersion,  $\sigma$ , of greater than 500 km s<sup>−1</sup> are therefore assumed to be broadline Seyferts (Type 1 AGN), and due to the relatively low number of these (less than 4

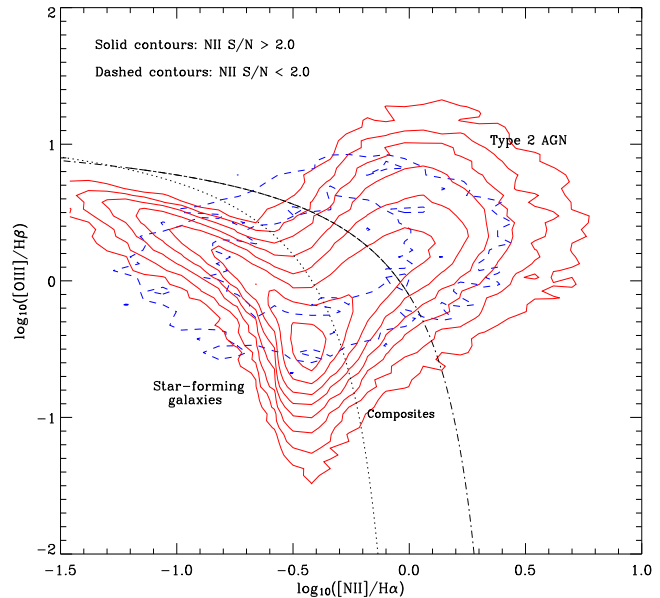


**Figure 1.** BPT diagnostic diagram for DR4 SDSS galaxies, showing the distributions of the sample, above and below our  $S/N$  cut of 2.0. The dot-dashed line is the Kew01 maximum star-burst line. The dotted line is the Kauf03 classification line.

per cent of the overall sample), are rejected from this analysis. In this paper therefore, we will only be comparing inactive galaxies with narrow-line galaxies (‘Type 2’ AGN, or ‘Type 2’ Seyferts). Exclusion of type 1 AGN from our active sample does not affect the overall conclusions.

The MPA DR4 catalogue contains derived physical properties for 567 486 galaxy spectra of 520 738 individual galaxies, with duplicates being removed using a 1.5'' matching radius. A redshift cut of  $0.01 < z < 0.16$  is then applied to all galaxies to limit evolution,  $k$ -corrections, and low-redshift problems. 359 154 DR4 galaxies then remain in our sample, from which active galaxies are isolated, leaving most of the remaining galaxies to be used as potential control galaxies. Once the AGN sample has been produced, two inactive control galaxies are selected for each AGN, closely matched in their optical properties.

### 3.1 AGN and Inactive Classification

In order to compare active and inactive galaxies, the SDSS galaxies must be classified and the AGN separated out. Baldwin et al. (1981), hereafter BPT, demonstrated that it is possible to distinguish Type 2 AGN from normal star-forming galaxies using the relative intensity ratios of easily-measured emission lines. BPT found that the most useful intensity ratios were  $[OIII]/H\beta$ ,  $[NII]/H\alpha$ ,  $[SII]/H\alpha$  and  $[OI]/H\alpha$ , and plotting these ratios against each other yields diagnostic diagrams.

These emission lines have been accurately measured for all DR4 galaxies, as described by Tremonti et al. 2004. The SDSS spectroscopic pipeline performs only a simple estimate of the stellar continuum, which is good for strong lines, but not for weaker emission lines. The Tremonti et al. pipeline on the other hand, estimates the stellar continuum by taking account stellar Balmer absorption, and hence recovers

<sup>1</sup> Data publicly available at <http://www.mpa-garching.mpg.de/SDSS/DR4/>

weaker nebular emission line features. This allows for a more accurate classification scheme of SDSS galaxies.

We adopt a similar classification scheme to that devised by Brinchmann et al. (2004), who split the sample into three main classes of galaxies based on their positions in the various BPT diagrams. These classes were defined to be star-forming or passive galaxies, AGN, and composite galaxies. Two extra sub-samples were derived for low signal-to-noise star-forming galaxies, and low signal-to-noise AGN. A final class was designated to ambiguous galaxies whose position in the various BPT diagrams appeared to place them in more than one class - this class most likely to be made up of galaxies with weak or no emission lines.

For our purpose, it is sufficient to separate ‘active’ and ‘inactive’ galaxies. We therefore split the sample into three classes - star-forming/passive galaxies, Type 2 AGN, and composite galaxies. We also use the Kewley et al. 2001 (hereafter Kew01) maximum star-burst separation line (dot-dashed line in Fig. 1) and the Kauffmann et al. 2003b (hereafter Kauf03) demarcation line (dotted line in Fig. 1) to select our sample. Therefore, in this study, a galaxy is defined to be a **Type 2 AGN** if

$$\log([OIII]/H\beta) > 0.61/(\log([NII]/H\alpha) - 0.05) + 1.3 \quad (1)$$

or defined to be a purely **star-forming galaxy** if

$$\log([OIII]/H\beta) < 0.61/(\log([NII]/H\alpha) - 0.47) + 1.19. \quad (2)$$

where [OIII] refers to the [OIII]  $\lambda 5007$  emission line, and [NII] is the [NII]  $\lambda 6584$  line.<sup>2</sup> Galaxies that fall in between these classification lines are galaxies that are classified as AGN according to the more lenient Kauf03 separation line. These galaxies are kept as the separate class of **composite galaxies**, as per Kauf03.

We tested the sensitivity of our results to the galaxy classification, by slightly altering equations (1) and (2) in our selection process, making the composite sample smaller. The effects of such changes were minimal, so for simplicity, and comparison with other results, we continued to use the Kew01 and Kauf03 separation lines.

The Type 2 AGN and composite galaxies were also subjected to a signal-to-noise cut, to ensure reliable AGN classification. We chose to cut at  $S/N > 2.0$  in the [NII]  $\lambda 6584$  emission line. As the [NII] emission line flux for star-forming and passive galaxies can be low, no  $S/N$  cut was required for that classification. Figure 1 shows a BPT plot for the overall DR4 sample. We have plotted the sample in two  $S/N$  bins. The solid contours show the distribution of galaxies with  $S/N > 2.0$ , while the dotted contours show the distribution of those with  $S/N < 2.0$ . The latter distribution shows that these low  $S/N$  galaxies are randomly distributed across the whole BPT diagram, so will not accurately represent AGN. Above a  $S/N$  of two, the BPT diagram takes its familiar form, so although this is a loose constraint it is still a reasonable cut for our statistical purposes in this paper, and allows us to keep the weaker AGN. A stricter cut of  $S/N > 3.0$  was also tried, and found to have little impact

<sup>2</sup> When calculating the logarithms in Eqns. 1 and 2, for each line flux, the value used is the higher of the measured line flux and its 1-sigma uncertainty. This avoids anomalously large, small or negative line ratios when one or both lines are undetected.

**Table 1.** Basic sample data following classification

Subsample	Number	Percentage
All galaxies ( $0.01 < z < 0.16$ )	359 154	100.0
SF + Passive	176 596	49.2
Type 2 AGN ( $S/N > 2$ in [NII])	69 783	19.4
Composites ( $S/N > 2$ in [NII])	64 136	17.9
Type 1 AGN (reject)	13 331	3.7
Unclassified (reject)	35 308	9.8

on the overall results. Table 1 summarises the numbers of galaxies classified and rejected for our analysis.

Typical [OIII] luminosities in our active sample range from  $10^5 L_\odot$  to  $10^8 L_\odot$ . The mean luminosity is approximately  $10^6 L_\odot$ : the majority of active galaxies would be considered to be ‘weak AGN’ (Kauffmann et al. 2003c) as less than 10% of the active sample has  $L[OIII] > 10^7 L_\odot$ .

### 3.2 Control Galaxy Selection

In order to perform a comparative study of active and inactive host galaxies, careful selection of inactive control galaxies is required. Control matching is critical because the AGN classification is strongly dependent on aperture effects, which can be minimised by matching redshift, and inclination, which can be minimised by matching on aspect ratio. We also want to match to galaxies of a similar size and luminosity. Therefore, for each of the active galaxies we selected two inactive galaxies, closely matched in the following properties:

- (i) Redshift,  $z$ , where  $0.01 < z < 0.16$  (AGN and composites restricted to  $0.02 < z < 0.15$ );
- (ii) Absolute  $r$ -band magnitude,  $M_r$ ;
- (iii) Aspect ratio,  $b/a$ , (Isophotal minor/major axis ratio in  $r$ -band);
- (iv) Radius,  $petroR90$  (in arcsec), containing 90% of the Petrosian flux, averaged over  $r$ - and  $i$ -bands.

Isophotal major and minor axis values, given by *isoA* and *isoB* respectively, are from the SDSS pipeline **frames**. **frames** measures the radius of a particular isophote of the galaxy, as a function of angle, and then Fourier expands this function. It then extracts *isoA* and *isoB* from the resulting coefficients. This is done in all wavebands, but only the  $r$ -band values were used in this analysis. *petroR90* is also obtained through the **frames** pipeline. This calculates the radius containing 90% of the Petrosian flux for each band. At this stage *petroR50* is also derived, which is the radius containing 50% of the Petrosian flux.

The  $r$ -band absolute magnitude used in this paper is given by

$$M_r = r - k_r - 5 \log(D_L/10 \text{ pc}) \quad (3)$$

where  $r$  is the Milky-Way-extinction-corrected Petrosian magnitude,  $D_L$  is the luminosity distance for a cosmology with  $(\Omega_m, \Omega_\Lambda)_0 = (0.3, 0.7)$  and  $H_0 = 70 \text{ km s}^{-1} \text{ Mpc}^{-1}$ , and  $k_r$  is the  $k$ -correction using the method of Blanton et al. (2003b).<sup>3</sup>

<sup>3</sup> The  $k$ -corrections were derived from **kcorrect v. 4.1.3**.

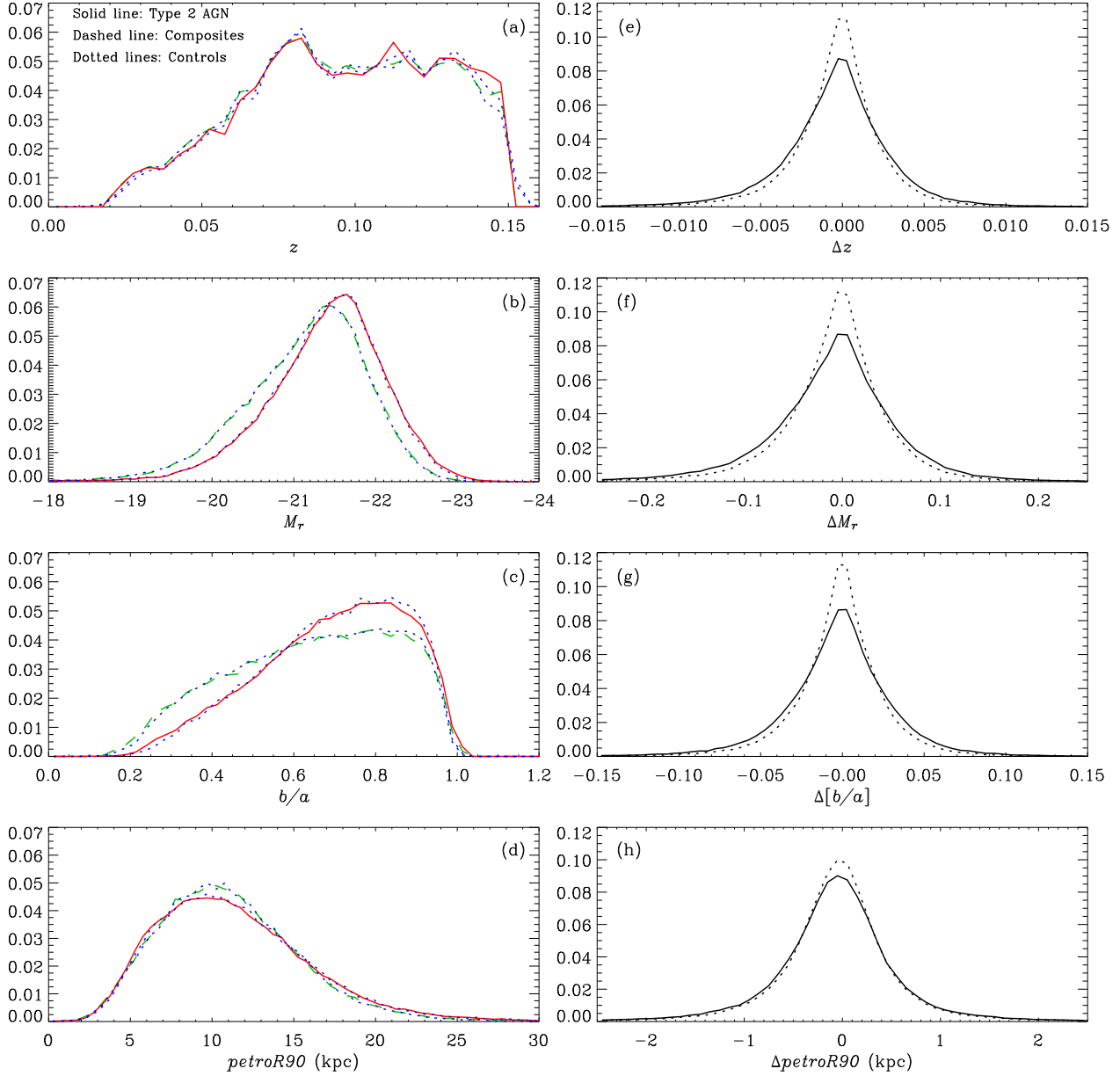


**Figure 2.** Left-hand side: Normalised distributions of (a) redshift, (b) absolute magnitude, (c) aspect ratio, and (d)  $petroR90$  radius, for our AGN (solid red lines) and composite galaxies (dashed green lines), along with their matched controls (dotted blue lines). Right-hand side: Normalised histograms of the individual differences between AGN/composites and each of their controls. The best controls are represented by the dotted lines, the 2nd best controls by the solid lines.

Two controls were selected for an AGN by calculating the differences,  $\Delta z$ ,  $\Delta[b/a]$ ,  $\Delta M_r$ ,  $\Delta petroR90$ , between the AGN and each control. The differences were then weighted, and summed as follows:

$$\Delta C = \frac{|\Delta z|}{0.01} + \frac{|\Delta M_r|}{0.2} + \frac{|\Delta[b/a]|}{0.1} + \frac{|\Delta petroR90|}{0.2''} \quad (4)$$

The two controls with the lowest values of  $\Delta C$  were then selected, and added to the controls catalogue. This was done for all Type 2 AGN, and then done separately for all composite galaxies. The weightings were such that we constrained the redshift and absolute magnitude more tightly than the other two parameters [see Fig. 2(e-h)].

### 3.3 Sample Distributions

The classification and control matching results in 2 pairs of galaxy catalogues: an AGN catalogue of 64 584 Type 2 AGN according to the Kew01 criteria (inclusive of LINERs), along with a catalogue of 129 168 control galaxies (Controls A); and a catalogue of 60 038 composite galaxies, with a matched set of 120 076 control galaxies (Controls B).

The resulting overall distributions of the selection properties are displayed in Fig. 2(a-d), along with the overall distributions of the differences in these properties between the AGN/composites and each of their two controls - Fig. 2(e-h). The best controls (dotted lines) result in a sharper peak

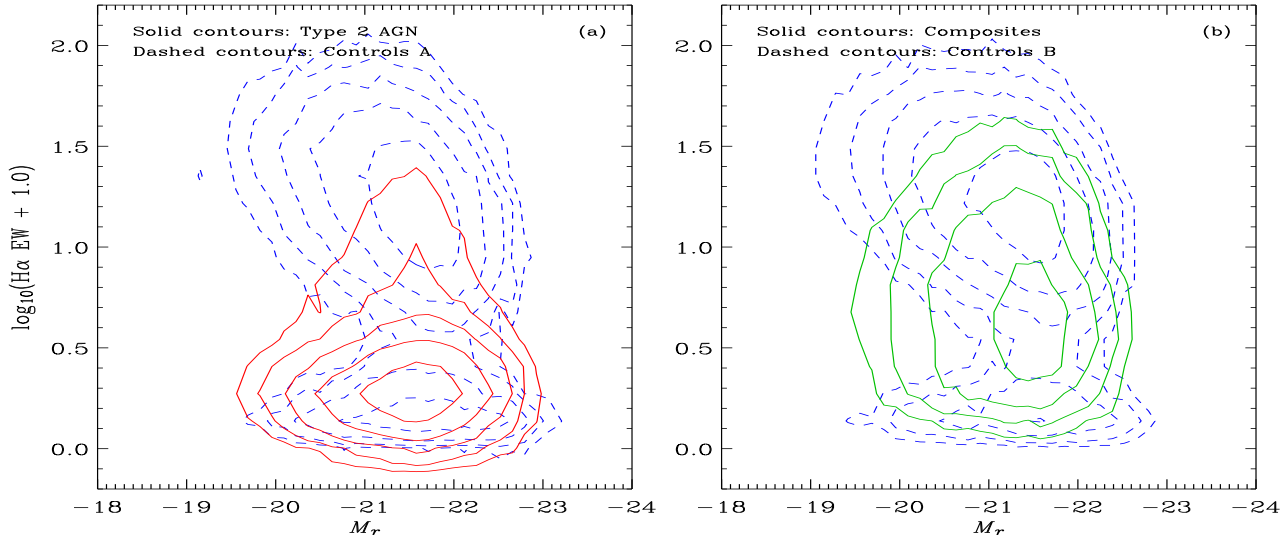


**Figure 3.** Observed distribution of  $H\alpha$  equivalent width vs. absolute magnitude. The contours are determined for galaxy number counts in  $0.135 H\alpha \times 0.135 \text{ mag}$  bins. The contour levels are on a logarithmic scale, starting at 64 and doubling each contour. The solid lines in (a) are Type 2 AGN, and in (b) are composites. The dashed lines are the control galaxies in both cases.

in the distribution, while the second best controls in our selection — solid lines in Fig. 2(e-h) — show slightly broader wings. Control matching was done using all ‘inactive’ galaxies each time, so it is possible the same controls can be picked more than once, if they fit the selection criteria for multiple AGN. It was not appropriate to make all control galaxies unique, as this would introduce systematic errors in the control matching.

## 4 RESULTS

A significant feature in recent analyses of galaxy populations is the recognition that the distribution of rest-frame colours is bimodal (e.g., Baldry et al. 2004). There is a well-characterised red sequence of predominantly massive, passively evolving early-type galaxies, and a blue sequence of late type, star-forming galaxies. This is a key feature for understanding galaxy evolution, and here we extend this analysis to identify where active galaxies fit into this picture.

Past observations by, e.g., Treu et al. (2005), suggest that galaxies transition from the blue to the red sequence, in a manner consistent with “cosmic downsizing” (Cowie et al. 1996); mergers between gas-rich blue galaxies producing ellipticals, with a predicted phase of bright quasar activity which terminates star-formation, and hence leads to the galaxy becoming red.

### 4.1 Equivalent width–Magnitude relations

The Balmer  $H\alpha$  line is a clear indicator of active star formation (Kennicutt & Kent 1983), and hence is a good way of separating out the red and blue galaxy sequences (Balogh et al. 2004; Haines et al. 2007). Fig. 3(a) shows the distribution of the equivalent width (EW) of the  $H\alpha$  lines in our AGN sample and the Controls A sample, as a function of absolute  $r$ -band magnitude.

The galaxy bimodality is clearly observed in the distribution of control galaxies, with late-type, star-forming galaxies (blue sequence) occupying the top half of the plot, and early-type, passive galaxies falling at low  $H\alpha$  strength, and peaking at a slightly higher luminosity. The peak of the AGN population falls along the blue edge of the red sequence, i.e., shows increased  $H\alpha$  EW relative to inactive red-sequence galaxies. The composite galaxies, shown in Fig. 3(b), however, show the peak of their distribution is located in the valley between the blue and red sequences of the Controls B sample. Both these results suggest evidence for a “transition” population, supporting galaxy evolutionary theories, in which star formation in massive galaxies ceases due to the presence of an AGN, resulting in a migration from the blue sequence to the red sequence. (Note that there is no requirement that AGN or composites have significant  $H\alpha$  emission, only  $NII S/N > 2$  is required).

### 4.2 Colour–Magnitude Relations

$g - r$  colour reflects a longer timescale of star formation compared to  $H\alpha$ , which is more representative of instantaneous star formation (or AGN-heated nebular emission). The colour-magnitude diagrams for our SDSS sample are shown in Figure 4. The left-hand side plot again shows the Type 2 AGN and Controls A, while the right-hand panel shows the composite galaxies with Controls B. The bimodality of colours can be seen in the distributions of control galaxies in both cases. From the CMD in Fig. 4(a), the majority of AGN now appear to reside along the peak of the red-sequence, rather than along its blue-edge. The AGN population does, however, still extend to the red edge of the blue sequence as well.

The location of the composite galaxies is less conclusive in this case [Fig. 4(b)]. The peak of this population is not so clearly just in between the red and blue sequences, as was the case in the  $H\alpha$  plot, but rather shows a more extended,



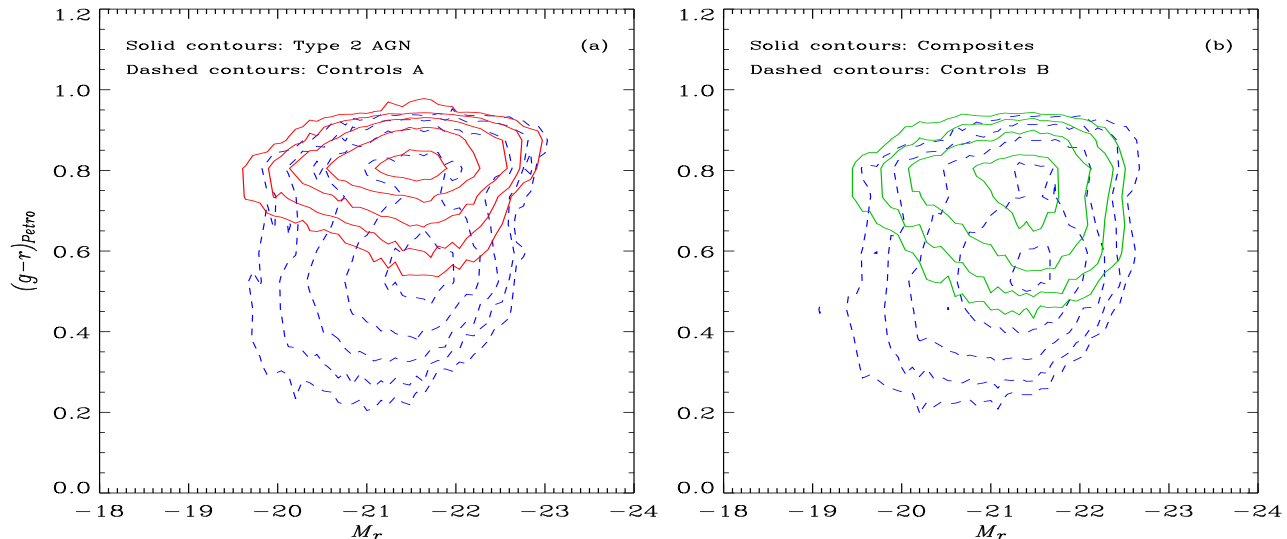


**Figure 4.** Observed distribution of colour vs. absolute magnitude, for (a) Type 2 AGN, and (b) composite galaxies, and their respective controls. The contours are determined for galaxy number counts in  $0.1 \text{ colour} \times 0.06 \text{ mag}$  bins. The contour levels are on a logarithmic scale, starting at 16 and doubling each contour. The solid lines represent the ‘active’ galaxies, while the dashed lines are the control galaxies.

irregular distribution. The distribution tracks the red sequence, in a manner similar to that of the AGN sample, but also extends to much bluer colours, indicating ongoing star formation, but with AGN activity also taking place. This result suggests that the composites do not necessarily represent a transition population, as implied by Fig. 3(b).

#### 4.3 Colour-Concentration Relations as a function of $M_r$

Although we have demonstrated that the galaxy population separates into red and blue sequences, this does not take into consideration the structure or morphology of galaxies. A robust method of outlining the sequences is to consider a joint distribution in colour and structure (Driver et al. 2006). Figure 5 shows the distribution of observed galaxies in colour versus concentration index for six different absolute magnitude ranges.

The inverse concentration index, given by  $C = \text{petroR50}/\text{petroR90}$ , has been used in our analysis. For typical galaxies,  $C$  ranges from 0.3 (concentrated) to 0.55; for comparison, a uniform disk would have  $C = 0.75$ .

In the distribution of the control galaxies (Controls A; Figure 5), the peak of the red sequence gets slightly redder (0.75 to 0.90) and more concentrated (0.38 to 0.32) with brighter magnitude, while the blue sequence also gets redder (0.45 to 0.60) but at an approximately constant concentration index of 0.45. At fainter magnitudes ( $-18 > M_r > -19$ ) there are few control galaxies on the red sequence, and there is just a blue, low-concentration cloud. At brighter magnitudes, it is the blue sequence that begins to disappear, with only the red sequence clearly defined. The AGN population peaks in approximately the same place as the peak of the red sequence for the control sample, hence also gets redder and more centrally concentrated with brighter magnitude.

Figure 6 shows the colour-concentration relations for

the sample of composite galaxies, along with Controls B. The distribution of Controls B varies in the same way as Controls A in Fig. 5, but the composite galaxies show a slight difference to the Type 2 AGN. The peak of the composite population again becomes more centrally concentrated with increasing magnitude, but there is almost no change in colour. A more complex morphology in the peak of the composite distribution also emerges in the range  $-20 > M_r > -23$  [Fig. 6(c-e)], which is inconsistent with a simple transition population implied by Fig. 3(b).

#### 4.4 Colour-Environment Relations as a function of $M_r$

The relationship between galaxy colour and environment can also add constraints to the processes involved in galaxy evolution. In this section we investigate the variation of the projected neighbour density  $\Sigma$ , with  $g-r$  colour and absolute magnitude.

Environmental densities were determined for SDSS galaxies by Baldry et al. (2006), using the projected distance to the  $N$ th nearest neighbour that is a member of a density defining population (DDP). The DDP were galaxies with  $M_r < -20$ . For each galaxy,  $\Sigma$  was determined from the 4th and 5th nearest DDP galaxies within  $\Delta z = 1000 \text{ km s}^{-1}$ . The environment measurements were only reliable to  $z < 0.085$  so our sample sizes were reduced to 22 747, 21 666, 44 592 and 42 966, for Type 2 AGN, composites, Controls A and Controls B, respectively. This also included a modest rejection of galaxies whose density measurements were highly uncertain.

Figure 7 shows how mean galaxy environment varies with colour and absolute magnitude. The top row shows the AGN sample and Controls A, while the bottom row shows the composites and Controls B. We have plotted the mean  $\log \Sigma$ , in colour bins of 0.05, for three magnitude ranges. We

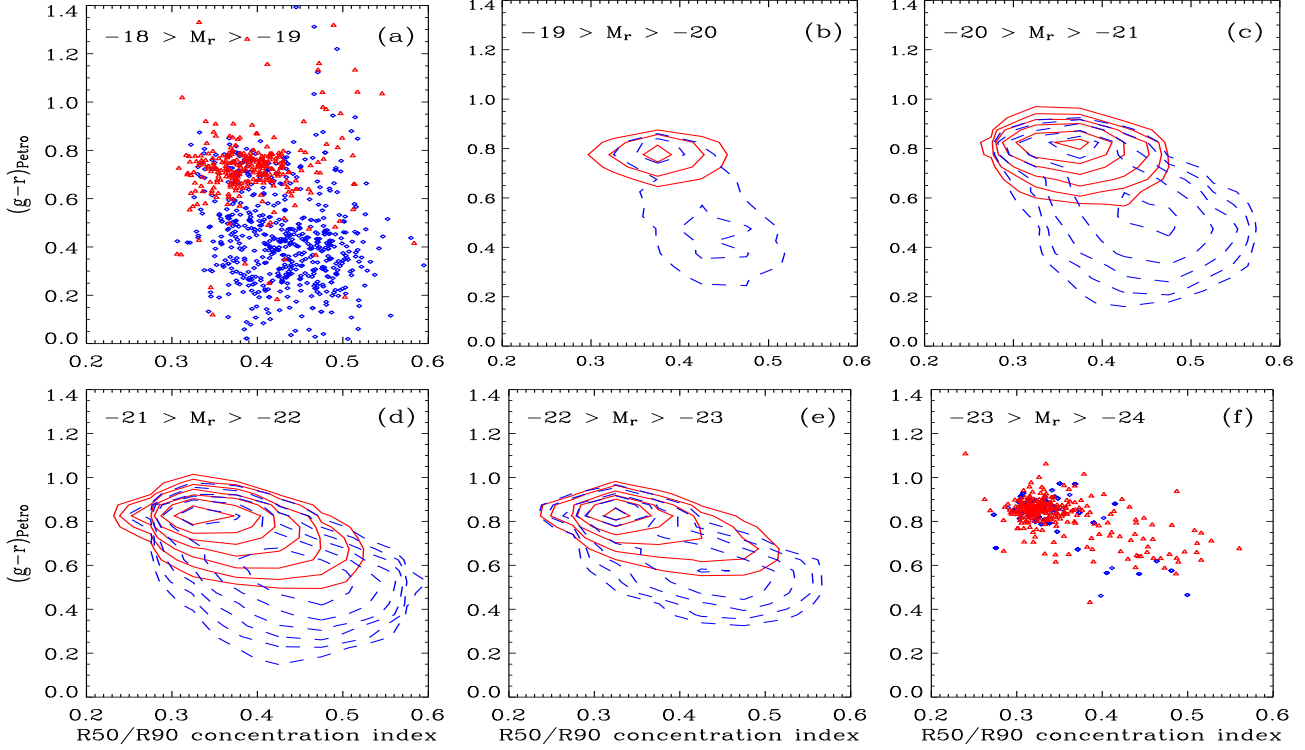


**Figure 5.** Colour vs. concentration index for different luminosity ranges. The contours are determined in  $0.05 \text{ colour} \times 0.05 \text{ concentration}$  bins. The contour levels are on a logarithmic scale, starting at 64 and doubling each contour [Plots (a) and (f) had insufficient numbers for contours]. The solid red lines/red points are Type 2 AGN, and the dashed blue lines/blue points are ‘Controls A’ galaxies.

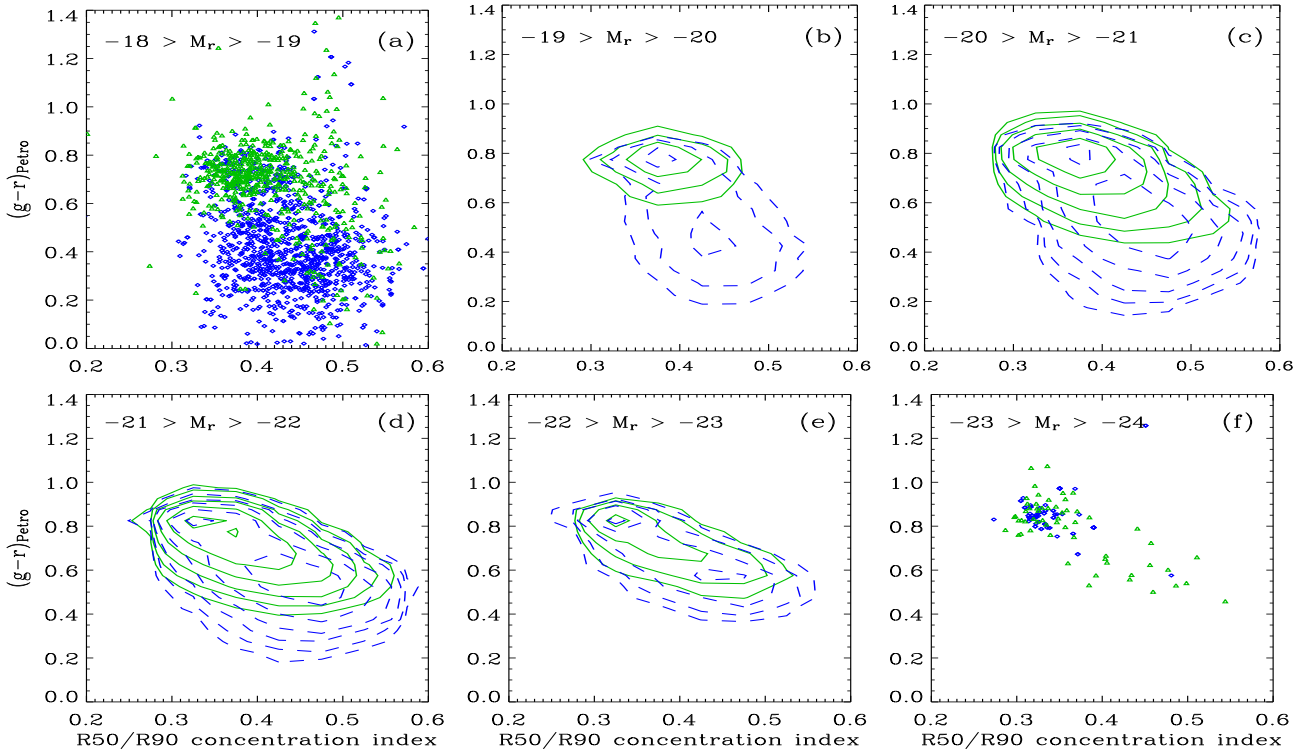


**Figure 6.** Colour vs. concentration index for composite sample, in stellar-mass bins of  $1 M_\odot$ . The solid green lines/green points are composites, and the dashed blue lines/blue points are ‘Controls B’ galaxies. See Fig. 5 for details.



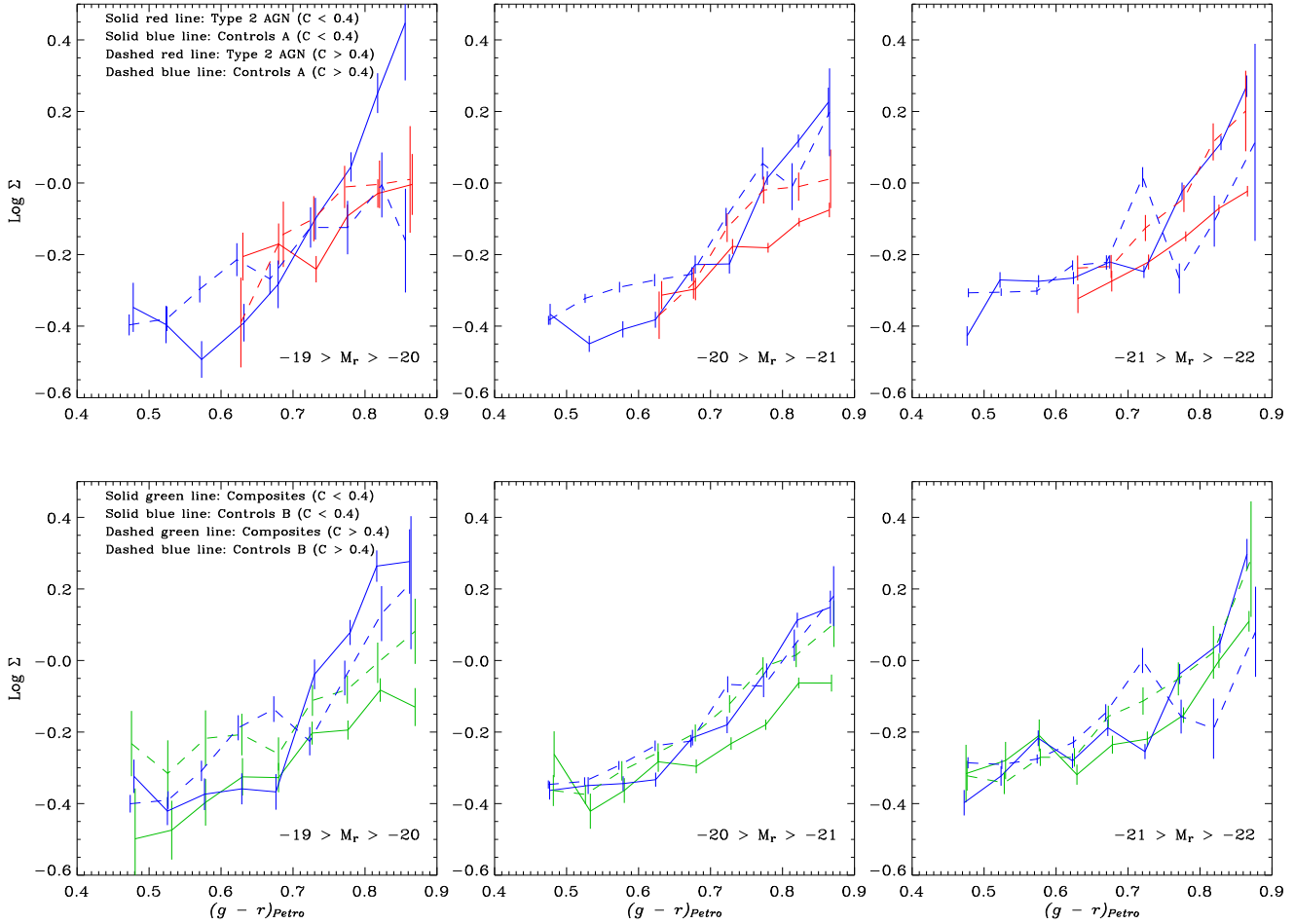


**Figure 7.** Mean  $\log \Sigma$  versus  $(g - r)_{Petro}$  colour, for three magnitude bins. Top row: Type 2 AGN sample compared to Controls A. Bottom row: Composites compared to Controls B. In both cases solid lines represent nominally bulge-dominated systems ( $C < 0.4$ ), while dashed lines represent more disc-like systems ( $C > 0.4$ )

have also further split these up into two concentration bins;  $C < 0.40$  (nominally bulge-dominated galaxies; solid lines), and  $C > 0.40$  (nominally disc galaxies; dashed lines).

From Fig. 4, a simple colour divide between the red and blue sequences occurs at  $(g - r)_{Petro} = 0.7$ . Below 0.7 lie mainly late-type galaxies, and above 0.7 are the early-type galaxies. Generally speaking then, Fig. 7 shows that late-type galaxies occur in less dense environments, while an increase in colour across to the red sequence coincides with more dense environments. Comparing just the solid lines in Fig. 7 — i.e., bulge-dominated systems — suggests that on the red sequence, inactive galaxies occur in more dense environments than active galaxies — Type 2 AGN or composites. This effect is also stronger at fainter magnitudes. In contrast, galaxies with  $C > 0.4$  show little difference in environment density across the different classes of galaxy, but all still show an increase in density with increasing colour.

At bluer colours, the error bars are greater as there are generally fewer late-type galaxies. Since AGN are also predominantly red, there is little reliable data for this class at  $(g - r)_{Petro} < 0.6$ .

Figure 8 shows the distributions of  $\log \Sigma$ , for galaxies with  $-19 > M_r > -22$ . The top panel consists of galaxies

with  $(g - r)_{Petro} > 0.7$  and  $C < 0.4$ , so predominantly concentrated red galaxies, while the bottom panel shows the distribution for galaxies with  $0.5 < (g - r)_{Petro} < 0.7$  and  $C > 0.4$ . There is little or no difference in the distribution of  $\log \Sigma$  across the various galaxy classes for the bluer, disc galaxies (bottom panel), with all populations favouring less-dense environments, with a peak at  $\log \Sigma = -0.5$ .

For the concentrated red galaxies, however, this is not the case. As in Fig. 7, we again see that AGN hosts favour less dense environments, but this time we also see a slight bimodality in the environments of inactive control galaxies. There is one peak, which falls in line with the peaks of the AGN and composite populations, which is again at  $\log \Sigma = -0.5$ , but there is also a secondary peak at a higher density of approximately  $\log \Sigma = 0.75$ , which most likely corresponds to a unique population of galaxies in higher density environments.

## 5 DISCUSSION

Having conducted a robust classification of ‘active’ and ‘inactive’ galaxies based on their emission line properties and

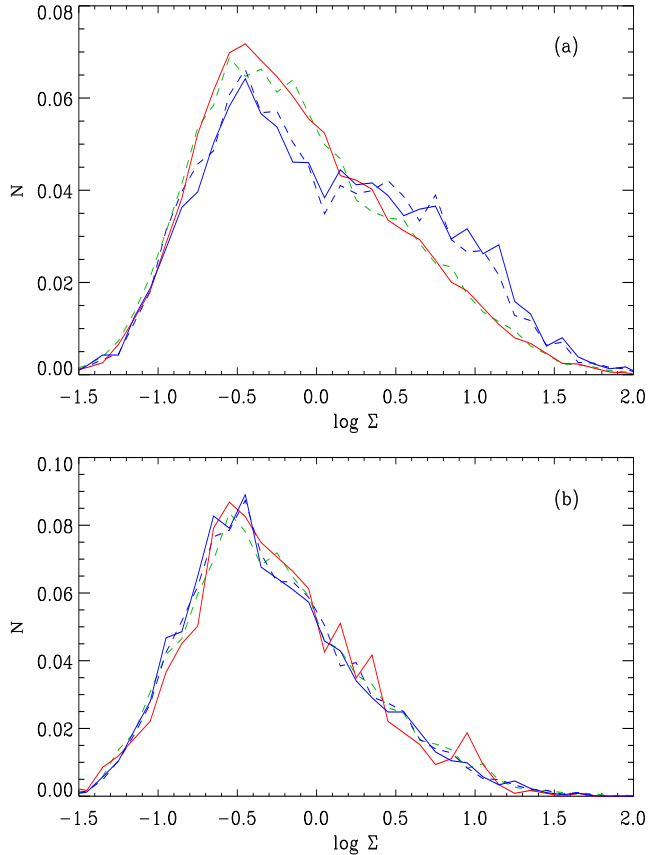


**Figure 8.** Top panel: Normalised distribution of  $\log \Sigma$  for galaxies with  $(g-r)_{\text{Petro}} > 0.7$  and  $C < 0.4$  (red sequence). Bottom panel: Normalised distribution of  $\log \Sigma$  for galaxies with  $0.5 < (g-r)_{\text{Petro}} < 0.7$  and  $C > 0.4$  (blue sequence). Solid red lines are Type 2 AGN, and solid blue lines are Controls A, while dashed green lines are composites, and dashed blue lines are Controls B.

locations in the BPT diagram, we have created an AGN catalogue, with a carefully selected control catalogue; and a catalogue of composite galaxies with another separate sample of well-matched control galaxies. The control galaxy samples both display a bimodal distribution in rest-frame colour, and also H $\alpha$  line strength. There is an AGN sequence that peaks along the red sequence and extends down to the red edge of the blue sequence. Composite galaxies appear to be slightly less luminous, and bluer, with the peak of the distribution possibly in the valley between the red and blue sequences (see also Miller et al. 2003).

There are a number of possible explanations for this result: one interpretation is that star formation maintains nuclear activity — i.e., starburst winds are fuelling the central black hole (Nandra et al. 2007). However, the fact that the majority of our AGN lie on the red sequence, suggests a shorter timescale for star formation associated with nuclear activity. This then points in the direction of AGN activity suppressing star formation in massive galaxies (Springel et al. 2005; Hopkins et al. 2005). In this scenario, there needs to be an initial injection of gas to feed the AGN, and then over time the AGN actually terminates star formation. In the local universe, AGN feedback has been

suggested as a mechanism to explain the observed effects of star formation quenching (e.g., Bower et al. 2006). Gas expelled during the feedback is believed to cool and relax the central regions of the galaxy resulting in passive evolution of the host galaxy, with stellar winds fuelling the AGN. This theory could also account for the observed  $M_{\bullet} - \sigma$  relation.

This would then naively predict that galaxies in the process of AGN feedback would lie in the valley between the blue and red sequences, as they gradually reduce the amount of on-going star formation until they end up on the red sequence. However, the efficiency of AGN feedback must be considered here, as it is unlikely that every AGN is able to suppress star formation in the galactic bulge every time it ignites. It may be that feedback can only occur during a quasar phase, and not during periods of weak AGN activity. If this is the case, then the weak AGN would not be responsible for the galaxy appearing in a ‘transition’ region, and the star-formation, AGN and dynamical timescales in the nucleus are likely to be the important factors for these galaxies.

While we do find many galaxies in this ‘valley’, particularly in the composite sample, it is difficult to conclude that this is a transitioning population, because of the complex morphology of composites in the colour–concentration plane shown in Fig. 6. Composites appear to be either already on the red sequence, or on the red edge of the blue sequence with a distribution in concentration index that is consistent with them remaining in the blue population. Other than stellar populations informing us whether or not there is a black hole, there is no obvious correlation between colour–concentration and the ability to fuel a black hole.

Drory & Fisher (2007) explain galaxy bimodality in terms of two different types of bulges — classical bulges, which are dynamically hot systems, and “pseudobulges”, which are dynamically cold, disc-like structures. The different structures are then thought to be indicators of the galaxy’s evolution. Classical bulges form through violent relaxation during major mergers in early epochs, when the environment density was high, making them red today. In contrast, pseudobulges are considered disc-only galaxies that have not undergone a major merger since forming their disc, hence are much younger, and bluer. Fig. 5 supports this interpretation, and shows that AGN are generally classical bulge-dominated systems (E to Sa). This result, along with the  $M_{\bullet} - \sigma$  relation indicates that the SMBH correlates with the classical bulge component, and not the galaxy as a whole, although the role of the host galaxy in triggering and fuelling the nuclear activity can not be ignored.

Whilst Fig. 6 shows that the majority of composites are also bulge-dominated systems, there is also evidence for another population as well, which is again inconsistent with a transition population. However, making a typical blue-sequence, disk-dominated galaxy red, does not make it a ‘red-sequence’ galaxy, as the latter are typically more massive, more concentrated, and of earlier Hubble-type, so it cannot be assumed that AGN activity in a less massive, late-type galaxy, is turning it into a red-sequence galaxy.

It has long since been established that early-type (red-sequence) galaxies are more clustered than late-type (blue-sequence) galaxies (Dressler 1980), but in addition to this result, we now find that active galaxies, despite being as red as inactive early-type galaxies, do not occur in such dense

environments as their inactive counterparts. In other words, the fraction of AGN amongst the red-concentrated galaxies decreases in denser environments. This result appears in contrast to Miller et al. (2003) who found that the AGN fraction was constant with environment. However, the combination of the passive-galaxy AGN fraction decreasing while the passive fraction increases could maintain the constant AGN fraction over all galaxies. We also note that we use a significantly larger sample with carefully matched controls.

Li et al. (2006) studied the clustering of narrow-line AGN in the SDSS, and on scales between 100 kpc and 1 Mpc, conclude that AGN are preferentially located at the centres of dark matter halos. If this is the case, then a proportion of the inactive red-sequence galaxies could be explained as satellite galaxies in high density environments, which gives rise to the implied increased density shown in Fig. 7, and the secondary peak in Fig. 8(a). Fuelling of AGN could be restricted in high-density environments except for galaxies at the centres of dark matter halos.

## 6 CONCLUSIONS

We have carried out a robust classification of ‘active’ and ‘inactive’ galaxies in the SDSS, based on their emission line properties and locations in the BPT diagram. We have compared the active galaxies with well selected control galaxies matched in redshift, absolute magnitude, aspect ratio and radius. We find that:

- Type 2 AGN host galaxies occur mainly on the red sequence of the CMD, but show increased levels of  $H\alpha$  flux in their emission compared to inactive red-sequence galaxies (Fig. 3(a) and Fig. 4(a));
- A separate class of composite galaxies appears to peak on the blue edge of the red sequence on the CMD, whereas the peak of the  $H\alpha$  distribution places composite galaxies firmly in the valley between the blue and red sequences (Fig. 3(b) and Fig. 4(b));
- Colour-concentration relations, however, show a more complex, possibly double, morphology in the peak of the composite distribution, rather than being in a valley (Fig. 6);
- AGN (and composites) are found in less dense environments on average than matched inactive red-sequence galaxies. The more clustered inactive galaxies are likely to be satellite galaxies in high-density environments (Fig. 7 and Fig. 8).

The key to understanding this in more detail now lies in the dynamics of the central regions of galaxies, to understand what activates some galaxies, but not others.

## 7 FURTHER WORK

The motivation for the construction of the parent sample presented here is an ongoing detailed study of the 3D distribution and kinematics of gas and stars in active and inactive galaxies using the IMACS-IFU on the Magellan telescope. Equal numbers of low-redshift ( $z < 0.05$ ), high-luminosity Type 1 Seyferts and Type 2 Seyferts (which includes composites) are carefully selected by inspection of their SDSS

spectra to ensure that they have strong emission lines, particularly in [OIII]. Control galaxies are then matched to the AGN in a similar way to the method presented in §3.2, but instead of two controls being produced, 10 to 15 potential matches are produced, and the best is selected following further inspection the SDSS images and spectra of the controls. This work is an extension of the SAURON-IFU study of nearby active and inactive galaxies by Dumas et al. (2007).

The study of the characteristics of a large statistical sample (this paper) complements detailed kinematic studies of a well-selected, but necessarily smaller sample of galaxies, which can identify the physical mechanisms that drive the trends observed in the statistical sample, through detailed, spatially resolved studies of individual galaxy nuclei.

## ACKNOWLEDGMENTS

PBW acknowledges PPARC for a postgraduate studentship. CGM acknowledges financial support from the Royal Society. We thank Neil Nagar for observations and collaboration on the 3D survey, Phil James for useful discussions, and the anonymous referee for helpful comments that improved the paper.

We acknowledge NASA’s Astrophysics Data System Bibliographic Services, the IDL Astronomy User’s Library, and IDL code maintained by David Schlegel (idlutils), and Michael Blanton (kcorrect) as valuable resources. Data were taken from the SDSS catalogue provided by the MPA Garching Group. Funding for the SDSS Archive has been provided by the Alfred P. Sloan Foundation, the Participating Institutions, the National Aeronautics and Space Administration, the National Science Foundation, the U.S. Department of Energy, the Japanese Monbukagakusho, and the Max Planck Society.

## REFERENCES

- Adelman-McCarthy J. K., et al., 2006, *ApJS*, 162, 38
- Allen S. W., Dunn R. J. H., Fabian A. C., Taylor G. B., Reynolds C. S., 2006, *MNRAS*, 372, 21
- Baldry I. K., Balogh M. L., Bower R. G., Glazebrook K., Nichol R. C., Bamford S. P., Budavari T., 2006, *MNRAS*, 373, 469
- Baldry I. K., et al., 2004, *ApJ*, 600, 681
- Baldwin J. A., Phillips M. M., Terlevich R., 1981, *PASP*, 93, 5
- Balogh M., et al., 2004, *MNRAS*, 348, 1355
- Blandford R. D., Rees M. J., 1974, *MNRAS*, 169, 395
- Blanton M. R., et al., 2003a, *AJ*, 125, 2276
- Blanton M. R., et al., 2003b, *AJ*, 125, 2348
- Bower R. G., et al., 2006, *MNRAS*, 370, 645
- Brinchmann J., Charlot S., White S. D. M., Tremonti C., Kauffmann G., Heckman T., Brinkmann J., 2004, *MNRAS*, 351, 1151
- Cowie L. L., Songaila A., Hu E. M., Cohen J. G., 1996, *AJ*, 112, 839
- Cross N. J. G., et al., 2004, *MNRAS*, 349, 576
- Dressler A., 1980, *ApJ*, 236, 351
- Driver S. P., et al., 2006, *MNRAS*, 368, 414

- Drory N., Fisher D. B., 2007, ApJ, in press, arXiv:0705.0973
- Dumas G., Mundell C. G., Emsellem E., Nagar N. M., 2007, MNRAS, 379, 1249
- Ferrarese L., 2002, ApJ, 578, 90
- Fukugita M., Ichikawa T., Gunn J. E., Doi M., Shimasaku K., Schneider D. P., 1996, AJ, 111, 1748
- Gebhardt K., et al., 2000, ApJ, 543, L5
- González Delgado R. M., Heckman T., Leitherer C., Meurer G., Krolik J., Wilson A. S., Kinney A., Koratkar A., 1998, ApJ, 505, 174
- Grupe D., Mathur S., 2004, ApJ, 606, L41
- Gunn J. E., et al., 1998, AJ, 116, 3040
- Haines C. P., Gargiulo A., La Barbera F., Mercurio A., Merluzzi P., Busarello G., 2007, MNRAS, in press, arXiv:0707.1262
- Hao L., et al., 2005a, AJ, 129, 1783
- Hao L., et al., 2005b, AJ, 129, 1795
- Heckman T. M., Kauffmann G., Brinchmann J., Charlot S., Tremonti C., White S. D. M., 2004, ApJ, 613, 109
- Ho L. C., Filippenko A. V., Sargent W. L., 1995, ApJS, 98, 477
- Hogg D. W., Finkbeiner D. P., Schlegel D. J., Gunn J. E., 2001, AJ, 122, 2129
- Hopkins P. F., Hernquist L., Cox T. J., Di Matteo T., Robertson B., Springel V., 2005, ApJ, 630, 716
- Huchra J., Burg R., 1992, ApJ, 393, 90
- Kauffmann G., et al., 2003a, MNRAS, 341, 33
- Kauffmann G., et al., 2003b, MNRAS, 341, 54
- Kauffmann G., et al., 2003c, MNRAS, 346, 1055
- Kennicutt Jr. R. C., Kent S. M., 1983, AJ, 88, 1094
- Kewley L. J., Dopita M. A., Sutherland R. S., Heisler C. A., Trevena J., 2001, ApJ, 556, 121
- King A., 2003, ApJ, 596, L27
- Komossa S., Xu D., 2007, ApJL, in press, arXiv:0708.0256
- Kriek M., et al., 2006, ArXiv:astro-ph/0611724
- Li C., Kauffmann G., Wang L., White S. D. M., Heckman T. M., Jing Y. P., 2006, MNRAS, 373, 457
- Lilly S. J., Tresse L., Hammer F., Crampton D., Le Fevre O., 1995, ApJ, 455, 108
- Liske J., Lemon D. J., Driver S. P., Cross N. J. G., Couch W. J., 2003, MNRAS, 344, 307
- Lynden-Bell D., 1969, Nature, 223, 690
- Martin D. C., et al., 2007, ApJS, in press, ArXiv:astro-ph/0703281
- Mathur S., Grupe D., 2005, A&A, 432, 463
- Merritt D., Ferrarese L., 2001, ApJ, 547, 140
- Mihos J. C., Hernquist L., 1996, ApJ, 464, 641
- Miller C. J., Nichol R. C., Gómez P. L., Hopkins A. M., Bernardi M., 2003, ApJ, 597, 142
- Nandra K., et al., 2007, ApJ, 660, L11
- Pier J. R., Munn J. A., Hindsley R. B., Hennessy G. S., Kent S. M., Lupton R. H., Ivezić Ž., 2003, AJ, 125, 1559
- Rush B., Malkan M. A., Spinoglio L., 1993, ApJS, 89, 1
- Sarzi M., Allard E. L., Knapen J. H., Mazzuca L. M., 2007, MNRAS, in press, arXiv:0707.0651
- Schlegel D. J., Finkbeiner D. P., Davis M., 1998, ApJ, 500, 525
- Schmidt M., 1963, Nature, 197, 1040
- Springel V., Di Matteo T., Hernquist L., 2005, MNRAS, 361, 776
- Stoughton C., et al., 2002, AJ, 123, 485
- Strateva I., et al., 2001, AJ, 122, 1861
- Struck C., 1997, ApJS, 113, 269
- Tremonti C. A., et al., 2004, ApJ, 613, 898
- Treu T., Ellis R. S., Liao T. X., van Dokkum P. G., 2005, ApJ, 622, L5
- York D. G., et al., 2000, AJ, 120, 1579